Journal of Materials Chemistry

Cite this: J. Mater. Chem., 2011, 21, 7953

www.rsc.org/materials

PAPER

Nanocomposite thin films for miniaturized multi-layer ceramic capacitors prepared from barium titanate nanoparticle based hybrid solutions†

Theodor Schneller,*[a] Sandip Halder,[a] Rainer Waser,[ab] Christian Pithan,[b] Jürgen Dornseiffer,[c] Yosuke Shiratori,[d] Lothar Houben,[e] Narayanan Vyshnavi[f] and Subhasish B. Majumder[f]

Received 10th February 2011, Accepted 31st March 2011
DOI: 10.1039/c1jm10607d

In the present work a flexible approach for the wet chemical processing of nanocomposite functional thin films is demonstrated. Barium titanate (BTO) based nanocomposite thin films for future miniaturized multi-layer ceramic capacitors are chosen as model systems to introduce the concept of "hybrid solutions" which consist of stabile mixtures of reverse micelle derived BTO nanoparticle dispersions and conventional molecular precursor solutions of either the same (BTO:BTO) or a specifically different material such as zirconia (BTO:ZrO_2). While in the case of using BTO:BTO *hybrid solutions* an interesting mode of microstructure control is found, the use of BTO:ZrO_2 hybrid solutions with various BTO : ZrO_2 ratios leads to nanocomposite films. BTO:BTO *hybrid solutions* yield columnar grown films with excellent permittivities up to 1050 with a significantly reduced number of coating steps at 700 °C. Low values of the temperature coefficient of capacitance are realized in the BTO–ZrO_2 nanocomposite thin films. The observed dielectric behavior of these films is explained based on the formation of a core–shell type microstructure on the nanoscale. A detailed high resolution transmission electron microscopy study combined with Raman spectroscopy and X-ray diffraction gives evidence for the proposed BTO–ZrO_2 nanocomposite character of these thin films.

1 Introduction

The advent of portable electronic devices with a steadily increasing number of functions in the same available space necessitates the further miniaturization of multilayer ceramic capacitors (MLCC). State of the art MLCCs fabricated by conventional tape casting or screen printing techniques consist of a multitude of dielectric layers with an individual thickness down to ~1 to 3 μm separated by base metal electrodes (~300 to 500 nm thick) of Ni, Cu, *etc.*[1,2] Thereby the capacitance of a MLCC (C_{MLCC}) can be estimated using the following expression.[3]

$$C_{MLCC} = [\varepsilon_r \varepsilon_0 (n - 1)s]/t \quad (1)$$

Here ε_r is the relative permittivity of the dielectric layer, ε_0 is the permittivity of the free space, n is the number of dielectric layers, s is the overlap area of the internal electrodes, and t is the thickness of the dielectric layer. To increase the specific volume capacitance (F/mm^3), ceramic materials with large dielectric permittivity, a high number of dielectric layers (n), large overlapping internal electrode area (s) and with individual dielectric layers as thin as possible (small t) are recommended.[3] For the required miniaturization of MLCCs, however, the reduction of the individual dielectric layer thickness is the most promising approach,[4] since alternative thin film materials with higher permittivities than the chemically modified $BaTiO_3$ (BTO), which is typically used in industry, are hard to find. The increase of the number of layers would increase the dimensions of the MLCC again. However further down-scaling of the individual dielectric layers by conventional tape casting or screen printing techniques is becoming increasingly difficult and will reach a technical limit for an estimated minimum dielectric layer thickness of only several hundreds of nm.[5]

[a]*Institute of Materials in Electrical Engineering and Information Technology 2, RWTH Aachen, University of Technology, 52056 Aachen, Germany. E-mail: schneller@iwe.rwth-aachen.de; Fax: +49 (0)241 80 22300; Tel: +49 (0)241 80 27820*
[b]*Institute for Electronic Materials, Research Center Jülich GmbH, 52425 Jülich, Germany*
[c]*Institute for Chemistry and Dynamics of the Geosphere 2, Research Center Jülich GmbH, 52425 Jülich, Germany*
[d]*Department of Chemical System Engineering, The University of Tokyo, Tokyo, Japan*
[e]*Institute of Microstructure Research and Ernst Ruska-Centre for Microscopy and Spectroscopy with Electrons, Research Center Jülich GmbH, 52425 Jülich, Germany*
[f]*Materials Science Center, Indian Institute of Technology, 721 302 Kharagpur, India*

† Electronic supplementary information (ESI) available: Representative DTA and TGA plots of a microemulsion derived BTO precursor powder, X-ray diffraction pattern of a pure nanoparticle derived barium titanate thin film, FESEM image of the surface morphology of a pure nanoparticle derived BTO thin film, the surface and cross-sectional morphology of the BTO-20Z, BTO-40Z, and ZrO_2 films characterized by FESEM, frequency dispersion of the dielectric constant and loss tangents of BTO and BTO–ZrO_2 nanocomposite films, and voltage dependent dielectric constants of BTO and BTO–ZrO_2 nanocomposite thin films. See DOI: 10.1039/c1jm10607d

On the other hand typical physical or chemical thin film deposition techniques also have restrictions if one aims to increase the film thickness. The conventional chemical solution deposition (CSD)[6] technique is not an economical approach for manufacturing of MLCCs due to a very large required number of repeated coating–firing cycles.[7] The metallo-organic chemical vapor deposition (MOCVD) technique has also not been found to be very attractive due to economic reasons, process complexity as well as deterioration of the film quality with increasing number of coatings.[8] Hence novel processing techniques should be sought to deposit tailor-made dielectric layers in the mesoscopic thickness range of 300–800 nm for miniaturized and highly volume-efficient MLCCs.

Due to its large dielectric constant barium titanate and its doped or modified varieties (m-BTO) remain a popular choice also for future generations of MLCCs. However, for the commercial acceptance of BTO thin film based miniaturized MLCCs several materials related issues need to be addressed. Very important is the necessity to anneal the dielectric material under reduced oxygen partial pressures in order to prevent the oxidation of the metallic electrodes, if Ni or other transition metals, which are typically used in standard MLCC's, are applied. Another technologically relevant issue is the matter of fact that the dielectric constant of BTO single crystals as well as of bulk ceramics strongly depends on the temperature. The maximum dielectric constant is achieved near a phase transition (Curie point, $T_c \approx 130$ °C), where the tetragonal distorted and therefore ferroelectric crystal modification of $BaTiO_3$ transforms into a cubic and thus paraelectric polymorph. Naturally, for the fabrication of dielectric layer thicknesses in the mesoscopic range, very small grain sizes approximately in the order of one fifth of the layer thickness are required.[9–12] For such films the dielectric anomaly at the structural phase transition becomes broader showing a reduced dielectric constant and a shift of T_c towards considerably lower temperatures. Since ferroelectricity is a collective phenomenon, these size driven effects may play an important role, if the dimensions of the individual ferroelectric crystallites reach the range below 100 nm. In order to understand these scaling effects a number of partially controversial discussed experimental and theoretical studies have been performed.[9,13–16]

Basically such ferroelectric nanoparticles can be prepared by different ways.[17–19] A major difficulty and challenge in the processing of such fine powders generally remains in the successful dispersion into dielectric inks that can be deposited in layers as thin as possible.

Recently, however, we have reported that microemulsion mediated synthesis presents a very versatile and attractive method to synthesize BTO nano-particles as well as mesoscopic BTO films with excellent dielectric properties.[20] To date such synthesis methods, using reverse micelles as reaction pools, have been mostly used to prepare isolated nano-crystalline BTO powders with a narrow particle size distribution.[21–25] Reports on microemulsion based synthesis of BTO thin films, however, are scanty.[11]

In this work we present a novel approach to mesoscopic BTO based thin films, which relies on the wet chemical deposition of so-called *hybrid solutions*.[26] These *hybrid solutions* consist of stable mixtures of reverse micelle stabilized BTO nanoparticle dispersions (μE-BTO) and conventional molecular precursor solutions. Such nanocomposite solutions enable unique possibilities to adjust the microstructure and the physical properties. Combinations of either the same material or a specifically different material like ZrO_2 in order to generate a heterogeneity on the nanoscale of the finally crystallized perovskite films can be realized. In the former case an interesting way was found to control the microstructure evolution of pure BTO films leading to improved dielectric properties. On the other hand for zirconia modified BTO (BTO-Z) thin films (with zirconia fractions varying from 0.0 to 40.0 wt%) the temperature coefficient of capacitance (TCC) can be reduced. The reduction of TCC with increasing Zr content is explained in terms of the formation of core–shell type BTO grains with grain to grain composition fluctuation of the Ti : Zr ratio. The possible mechanism of the formation of such core–shell structures and their influence on the dielectric properties of the resulting films are also discussed.

2 Results and discussion

Stable BTO nanoparticle dispersions used in this work have been prepared by a quantitative sol–gel reaction of a bimetallic Ba-Ti-methoxide precursor with inverse aqueous micelles formed from the cationic surfactant *c*etyl*t*rimethyl*a*mmonium *b*romide (CTAB) (see the Experimental section). By this route a stable dispersion with a solid content of 5 wt% corresponding to 0.17 mol l^{-1} was obtained. It is interesting to note that directly after synthesis the resulting BTO nanoparticles are basically of amorphous nature, in contrast to crystalline nano-particles obtained using non-ionic surfactants.[20,27]

At first the behavior of the pure BTO nano-particle dispersion with regard to film and phase formation as well as the corresponding electrical properties was investigated. All films were prepared on standard platinized silicon substrates (Pt(100 nm)/TiO_x(15 nm)/SiO_2(450 nm)/Si). In order to increase the density of the pure μE-BTO derived films, *hybrid solutions* consisting of μE-BTO and conventional BTO precursor solutions (*con*-BTO) were studied. The required 0.17 mol l^{-1} *con*-BTO solutions were prepared by mixing barium propionate in propionic acid with a butanolic titanium tetrabutoxide solution, which was stabilized with two equivalents of acetylacetone.[28,29] In the second part of this study the attention is drawn on the core–shell type heterogeneity on the nanoscale of zirconia modified BTO films as mentioned in the Introduction.

Characteristics of microemulsion derived barium titanate films

In order to select a suitable heat treatment schedule for the deposited μE-BTO as well as zirconia modified barium titanate (BTO-Z) films, differential thermo-analytical and thermo-gravimetric (DTA/TG) measurements of the dried precursor powders (see ESI†) in conjunction with X-ray diffraction (XRD) analyses of these powders calcined at different temperatures were carried out. It has been found that around 115 °C an endothermic evaporation of associated free solvents takes place and that at temperatures of ~322 °C most of the other organic species which are originating from the microemulsion are removed in an exothermic reaction. Between 600 and 700 °C a broad exothermic signal points to the crystallization of the material accompanied with a weight loss of approximately 5%, which

could possibly be related to the decomposition of intermediately formed carbonates. Hence typically temperatures of 700–750 °C have been applied for the crystallization of the BTO based films. A Fourier transform infrared (FT/IR) spectrum of a BTO thin film annealed at 750 °C for 10 minutes in ambient oxygen (not shown) reveals the formation of strong absorption bands (corresponding to the formation of metal–oxygen bonds) below 750 cm^{-1}, giving evidence for the crystalline nature of the annealed films,[29] which is also confirmed by their XRD patterns (see ESI†). Interestingly the comparison of the slow scanned XRD patterns (2θ from 44 to 47°) of this BTO thin film and of a BTO powder prepared from the nanoparticle dispersion which was calcined at 800 °C for 2 h shows different features. The clear splitting of the (200) diffraction peak in the BTO powder confirms its tetragonal perovskite structure, while the singular (200) diffraction peak observed for the BTO thin films indicates a global pseudo-cubic perovskite structure. Characterization of the films by confocal micro-Raman scattering (Fig. 1), on the other side, clearly and unambiguously confirms a crystallographic structure with tetragonal distortion at least on the local scale. This is evidenced by the appearance of a pronounced band at 307 cm^{-1}, arising from the Raman active B_1 + E(LO + TO) lattice vibrations of the tetragonal unit cell.

From the cross-sectional SEM image (Fig. 2(a)) a fine grained homogeneous and apart from minute surface porosity relatively dense morphology of the diffusion furnace annealed BTO thin films is deduced. The average grain size was estimated from the surface micrograph (see ESI†) to be about 30 nm.

The dielectric properties of these BTO thin films (with submicron thickness and nanosize grains) were characterized as a function of frequency, dc bias voltage, and temperature and are tabulated in Table 1. In addition the dielectric properties of nanocrystalline films synthesized using other thin film deposition techniques are arranged in Table 2.

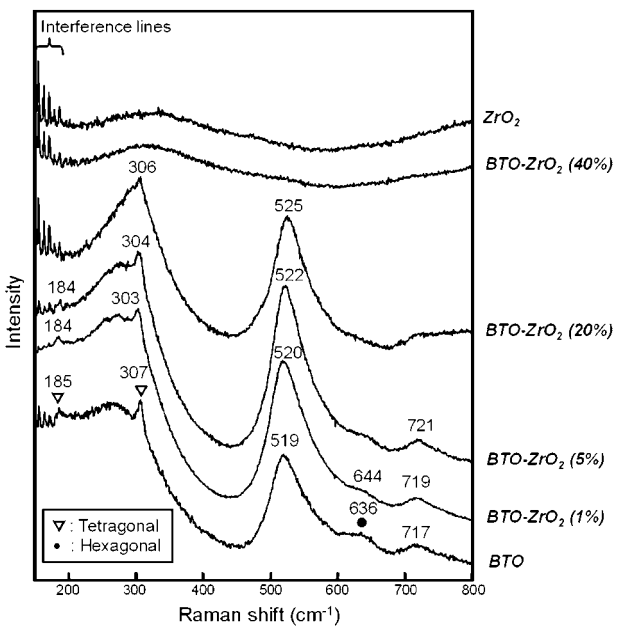

Fig. 1 Room temperature Raman spectra of $BaTiO_3$, ZrO_2 and $BaTiO_3$–ZrO_2 nanocomposite films.

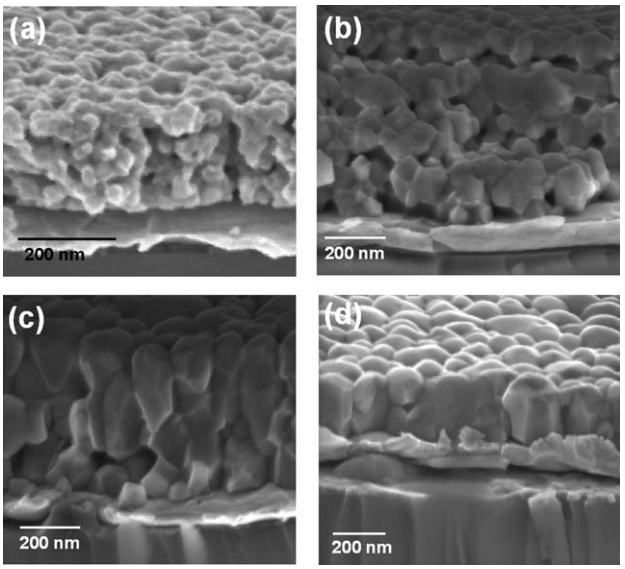

Fig. 2 Cross-sectional morphology of BTO thin films derived from different processes: (a) pure BTO-dispersion processed in a diffusion furnace (2 coating/firing cycles), (b) RTA processed pure BTO-dispersion (5 subsequent coating/firing cycles), (c) RTA processed dispersion with 20% of *con*-BTO additive (5 subsequent coating/firing cycles) and (c) RTA processed dispersion with 40% of *con*-BTO additive (5 subsequent coating/firing cycles).

Comparing Tables 1 and 2, it is apparent that excellent dielectric properties are achieved in micro-emulsion derived barium titanate thin films. This process therefore seems to be very promising in order to fabricate dielectric layers for miniaturized thin film MLCCs. Surveying several research reports on wet chemically synthesized barium titanate thin films, some general observations can be grouped as follows: (i) usually the grain size of the polycrystalline films with submicron thickness is in the nanosize regime (<100 nm). Films with a grain size in the nanoregime typically exhibit a broad dielectric anomaly corresponding to the tetragonal to cubic structural transition and often the transition temperature is significantly lowered as compared to single crystalline $BaTiO_3$ (~130 °C). (ii) The dielectric properties of BTO thin films depend on both their thickness as well as their grain size. There exists a critical grain size where BTO thin films are claimed to have a cubic or pseudo-cubic crystal structure even at room temperature. However, the published reports are inconsistent concerning the 'critical' grain size for $BaTiO_3$ and how exactly the critical size affects its dielectric as well as other electrical characteristics.[14] (iii) The annealing temperature at which the complete perovskite phase formation of CSD prepared BTO thin films occurs depends on the choice of precursor materials. When organic salts (barium acetate or other barium carboxylates) of barium are used along with titanium alkoxides as basis for the precursor solution, films often have $BaCO_3/TiO_2$ or $Ba_2TiO_5CO_3$ as intermediate products upon organic removal.[30–32] These carbonate rich intermediate phases have relatively high decomposition temperatures of approximately 650–700 °C and transform in this temperature range either through solid-state reaction between $BaCO_3$ and TiO_2[30,33,34] or by the decomposition of the oxo-carbonate intermediate[31] into the perovskite thin film. The latter pathway is

Table 1 Dielectric properties of microemulsion derived pure $BaTiO_3$ thin films

Physical quantity	Magnitude
Thickness of a single deposited layer upon annealing	*ca.* 0.120 μm
Total thickness	0.235 μm
Capacitor area	7.0×10^4 μm^2
Capacitance/volume (@1 kHz)	~65 μF mm^{-3}
Dielectric constant (ε) (@1 kHz)	~406
Loss tangent (@1 kHz)	1.3%
Change of dielectric constant (Δε/ε) with	
- Frequency (1 kHz to 200 kHz)	6%
- DC bias voltage (0 to + 10 V)	57%
- Temperature (−174 to +50 °C)	20%

observed in the case of the acetylacetone stabilized titanium alkoxide precursors and is expected to yield more homogeneous BTO films.[30] However recent works show that the formation of the intermediate carbonate rich phases is not the only reason for the relatively high crystallization temperature of BTO films and that there might be a lower limit of ~600 °C for this type of BTO film preparation.[35,36] While Halder *et al.*[35] avoided the formation of these carbonate rich phases by a 2-amino ethanol based precursor chemistry, Liedtke *et al.*[36] amorphized well crystalline (Ba,Sr)TiO_3 (BST) films by oxygen ion implantation and tried to recrystallize them subsequently. In both these cases no perovskite formation was observed below 600 °C.

In accordance with these works the *μE*-BTO derived films in the present study crystallize into the perovskite only above 600 °C as well. In summary these findings might be explained qualitatively by a certain activation energy which is needed for the crystallization of such amorphous films independent of the specific history of their preparation. Since in the case of the present cationic dispersion, the BTO nanoparticles are primarily amorphous after synthesis, the same temperature range is necessary to reorganize the ions into the crystalline perovskite structure.

Lower crystallization temperatures might be possible if inorganic compounds like barium halogenides or barium hydroxides are used. However in the first case reaction products in films annealed at low temperature may contain numerous complex oxides of the system BaO–TiO_2 along with oxo-halogenide compounds.[37] When barium hydroxides are used together with titanium alkoxide, formation of $BaTiO_3$ is also possible at a much lower annealing temperature. The formation mechanism of perovskite BTO is not fully understood. The Ti alkoxide is hydrolyzed to form a gel and probably Ba^{2+} ions (from the hydroxide) diffuse into the TiO_2 gel to form barium titanate at lower annealing temperature, in analogy to $BaTiO_3$ nanopowders prepared from similar precursors under hydrothermal conditions, for instance.[18] Although the crystallization temperature is lowered the hydroxyl ions have often been reported to deteriorate the dielectric properties of the resulting BTO films.[10]

In comparison to the above general problems for conventional CSD films, the microemulsion mediated synthesis route for BTO films has the following advantages. Firstly, films in the mesoscopic thickness regime can be prepared in a very time saving manner by only a few coating and firing cycles. As will be reported elsewhere, we have been able to deposit films as thick as ~2.5 μm by this technique (by only six coating/firing steps) which might be very useful for piezoelectric applications such as micro-electro-mechanical systems. Secondly, although nanoparticle dispersion derived BTO thin films crystallize into the perovskite structure at similar temperatures as optimized CSD solution derived films, the amount of undesirable barium carbonate is reduced to a minimum. FTIR spectra of the annealed BTO films confirm that these BTO films are free from any organic moieties or carbonate impurities. This was possible due to the special care which was taken to perform a controlled carbon dioxide free hydrolysis of the Ba-Ti-methoxide precursor within the reverse micelle water nano-pool. Thus the resulting amorphous BTO is confined inside the nano-reactors well dispersed due to the adsorbed surfactant in the oil matrix. Finally, and this might be the most important, the use of well dispersed BTO nanoparticles on the primary structure level in combination with dedicated conventional precursor solutions opens up a number of possibilities for the preparation of nanocomposite systems with improved electric properties. Two examples illustrating these possibilities will be presented in the following.

Table 2 Overview on processing conditions, morphology, and dielectric properties of nanocrystalline $BaTiO_3$-based thin films

			Morphology		Dielectric constants		
Material	Synthesis route	Process conditions	Thickness	Grain size	ε	tan δ	Ref.
$BaTiO_3$	Hybrid sol–gel and hydrothermal process	*Annealing*: 400–500 °C/5min and *hydrothermal process*: 180 °C/8 h	400 nm	25–35 nm[a]	80–205 (10 kHz)	>0.03 (10 kHz)	10
	Sol–gel[b]	*Annealing*: 700 °C/60 min and 750 °C/20 min	250–400 nm	~50 nm	117–127	0.02–0.05	12
	CSD	*Annealing*:[c] 750 °C/10 min	200 nm	200 nm[d]	900 (10 kHz)	—	31
	Microemulsion mediated route	*Annealing*: 800 °C	350 nm	20 nm	940 (1 kHz)	0.017 (1 kHz)	11
		Annealing: 800 °C/30–50 min	800 nm	50–70 nm	400 (1 MHz)	—	20
	Wet chemical process[e]	*Annealing*: dry: 300 °C, crystallise: 600 °C[f]	108 nm	20–30 nm	85–90 (1–100 kHz)	~0.03 (1–100 kHz)	9
$BaSr_{0.6}Ti_{0.4}O_3$	MOCVD (substrate: Pt–MgO)	*Annealing*: ~650 °C, O_2 *partial pressure*: 130–670 Pa and *deposition time*: 1–2 h	260 nm	—	250–1000 (1 kHz)	~0.022 (1 kHz)	8

[a] Before the hydrothermal process. [b] Deposition on the $LaNiO_3$ bottom electrode. [c] 22 deposition steps at 10 nm with 10 min annealing after each step. [d] Columnar microstructure—lateral diameter ~80 to 120 nm. [e] CSD of a bimetallic single-source precursor. [f] Properties of a film annealed at 850 °C were similar.

Films from BTO:BTO hybrid solutions

At first the improvement of the density of the pure nanoparticle dispersion derived BTO films is aimed. Therefore BTO:BTO hybrid solutions consisting of a mixture of the μE-BTO dispersion and various amounts (0 vol%, 20 vol%, and 40 vol%) of a conventional alkoxide/propionate based BTO precursor solution (*con*-BTO) have been synthesized. In the following these hybrid solutions and the respective films derived from them are referred to by the following nomenclature, in which *X*% *con*-BTO designates a solution or a film where *X* vol% of the original purely micellar solution was replaced by the conventional precursor solution.

The morphology of the BTO thin films is significantly changed compared to the conventional cases of purely CSD or micellar solution based depositions if the films are fabricated from *BTO:BTO hybrid solutions* by only a few sequential coating/crystallization steps. The cross-sectional field emission scanning electron micrographs (FESEM) of Fig. 2 show the evolution of the microstructure with varying *con*-BTO volume contents. Furthermore this figure shows by means of the pure μE-BTO derived films the effect of different annealing processes. While the diffusion furnace annealed (~10 K s^{-1}) films (Fig. 2(a)) show a similar microstructure to conventionally annealed CSD-films, the rapid thermally annealed (RTA) processed BTO films (~56 K s^{-1}) also have an equiaxed granular microstructure but with a larger fractured grain size (Fig. 2(b)). The microstructure features are changed significantly in RTA crystallized 20% *con*-BTO (Fig. 2(c)) and 40% *con*-BTO (Fig. 2(d)) containing hybrid solution derived BTO films. These films are dense and the formerly mentioned equiaxed granular structure obtained using the pure micellar solution is progressively transformed into a columnar granular structure upon the addition of *con*-BTO. It is interesting to note that the columnar microstructure is only achieved in rapid thermally annealed films and that similar hybrid films annealed in the diffusion furnace yield an equiaxed granular microstructure. Due to these different microstructures substantial differences in the dielectric constants have been measured (Fig. 3).

While in the case of the BTO films derived from pure microemulsions, the dielectric constant values are in principle comparable to those of the diffusion furnace processed films, the 20% and 40% *con*-BTO containing films show increased dielectric constants of around 910 and 1050, respectively (Fig. 3). At this point it is instructive to emphasize that the growth of columnar BTO films of similar thickness by standard CSD requires the fourfold coating effort, as reported previously.[31]

For commercial MLCCs the most widely used types are based on ceramic formulations meeting the Y5V and X7R specifications of the EIA (Electronic Industry Association).[3] Ceramic capacitors of the Y5V type exhibit a strong voltage and temperature dependence of capacitance whereas X7R type MLCCs exhibit a minimal frequency, temperature as well as voltage dependence of their capacitance values. As shown earlier,[20] for microemulsion derived pure barium titanate thin films, further material optimization is needed in order to reduce both the frequency and temperature dependence of the measured capacitance. The incorporation of a linear dielectric material in a non-linear dielectric matrix has been found to be efficient to

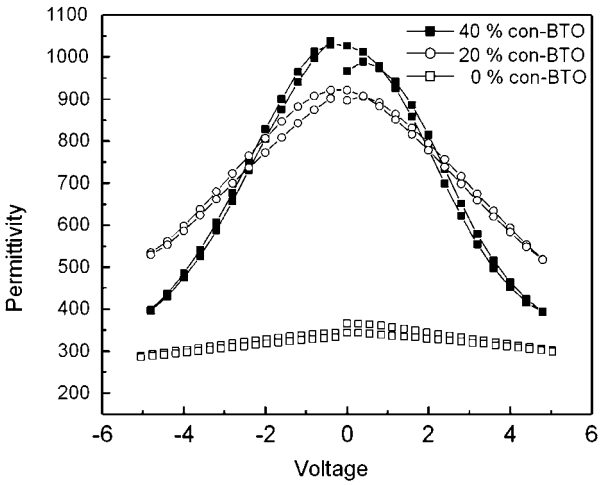

Fig. 3 Permittivity *versus* voltage of the RTA crystallized BTO:BTO *hybrid solution* derived thin films measured at 10 kHz. With increasing *con*-BTO content of the hybrid solution the films show a significant increase in the dielectric constant. The open squares represent the pure BTO nanoparticle dispersion, while the open circles and the filled squares represent the 20 vol% and 40 vol% *con*-BTO added thin films, respectively.

significantly reduce the frequency dispersion of the capacitance, loss tangent as well as leakage current densities. Realization of these effects strongly depends on the thin film geometry and the nature of dispersion of the low loss linear dielectric within the non-linear dielectric matrix.[38–40] Only a broad temperature dependent dielectric anomaly was obtained in these engineered thin film structures. For a significant reduction of the temperature coefficient of capacitance (TCC), local variation of the Curie temperature of barium titanate is essential. Substitution of Ti^{4+} cations in the BTO lattice by Zr^{4+} is known to reduce the paraelectric to ferroelectric phase transition temperature. However, it remains challenging to use this Curie point shifter cation to locally vary the transition temperatures (T_c) in order to achieve an almost flat temperature characteristic of the dielectric response.[4,40]

For engineering these properties *BTO:ZrO_2 hybrid solutions* with variable contents of alkoxide based zirconia precursor solutions (*con*-ZrO_2) have been synthesized and processed *via* CSD. For this purpose the required 0.17 mol l^{-1} *con*-ZrO_2 was synthesized by reaction of zirconium tetra-*n*-butoxide in butanol with 2 equivalents of acetylacetone (see the Experimental section). Hybrid solutions yielding in final composition with up to 40 wt% ZrO_2 were prepared. The resulting nanocomposite films are referred to as BTO-*x*Z, where *x* designates the content of ZrO_2 in wt%.

Structural properties of BTO–ZrO_2 composite films

The XRD reflections of the pure BTO, ZrO_2 and BTO–ZrO_2 (BTO-Z) composite films (Fig. 4) have been indexed to a pseudo-cubic perovskite structure whereas the zirconia films primarily crystallized into the monoclinic structure. From the Raman-measurements (Fig. 1) a phase assignment is quite difficult because of many overlapping bands. According to factor group

analysis[41] tetragonal ZrO_2 has 6 Raman active modes $A_{1g} + 2B_{1g} + 3E_g$, with characteristic peaks at 146, 270, 311, 457, 599, 649 cm^{-1}, respectively. The Raman active modes of the monoclinic modification are $9A_g + 9B_g$, some of them located at 178, 189, 222, 304, 333, 348, 380, 474, 503, 538, 611, 643 cm^{-1}.[42] In the case of cubic ZrO_2 only one single T_{2g} mode is observed. As marked by the arrow, an XRD peak of rather low intensity which corresponds to the tetragonal phase of ZrO_2 can also be identified. It is therefore conclusive that the alkoxide derived pure ZrO_2 thin films crystallize as a mixture of the monoclinic and tetragonal crystallographic polymorph. The coexistence of a tetragonal and a monoclinic phase has also been reported in the case of sol–gel derived zirconia powder calcined in the temperature range of 600–800 °C.[43] Several interesting features appear in the XRD-patterns of Fig. 4.

First, the individual peaks observed for zirconia are not identified in BTO-Z films with zirconia contents below 40%. Second, although the diffraction peaks become progressively broader with increasing Zr contents, no systematic peak shift of the (110) diffraction peak (most intense) can be observed upon

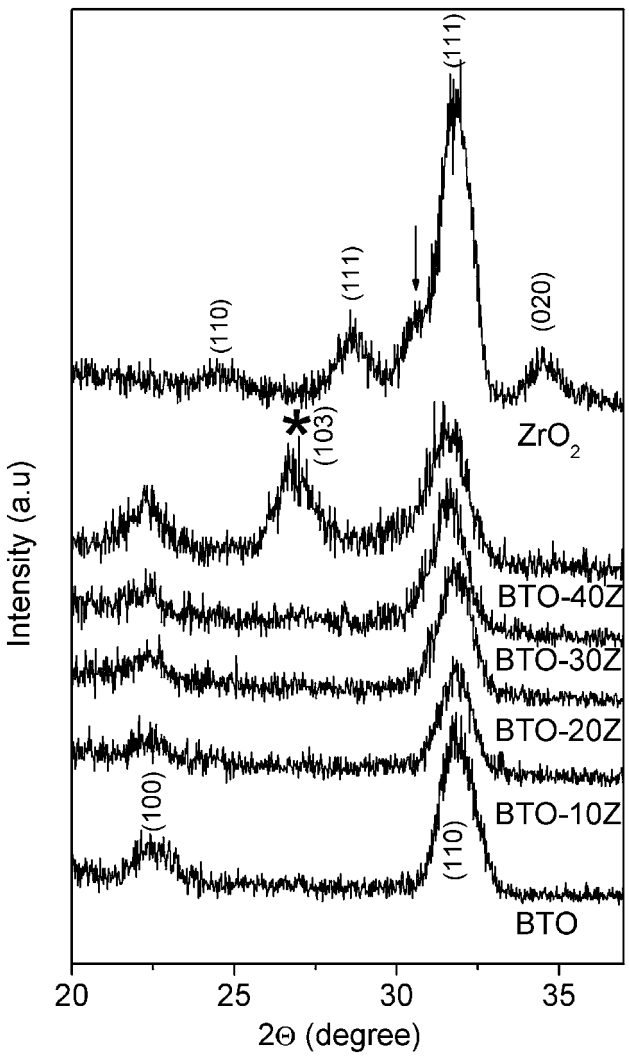

Fig. 4 Slowly scanned X-ray diffractograms of BTO, composite BTO–ZrO_2 and ZrO_2 thin films.

ZrO_2 addition. Finally, in BTO-40Z films, an XRD peak (marked by an asterisk) has been assigned to the (103) diffraction reflex of BTO with hexagonal symmetry. Usually for bulk ceramics the hexagonal phase of BTO crystallizes at a temperature as high as 1460 °C, however for soft solution processed nanocrystalline BTO, the appearance of this phase (at relatively much lower temperatures) has been suggested due to a locally stacked hexagonal sequence in the cubic/tetragonal matrix. The first observation indicates that ZrO_2 does not stay as a phase separated entity in the BTO matrix of the BTO-Z composite films. The second observation, on the other hand, indicates that with increasing ZrO_2 content there is no or only very little systematic incorporation of Zr^{4+} ions (with a definite Ti/Zr ratio) in the BTO lattice, which gives clear hints to heterogeneity on the nanoscale. Consequently no left shift of the diffraction peaks is observed with increasing Zr^{4+} content in contrast to true BTZ solid solution films prepared by conventional CSD processing of a standard propionate based BTZ coating solution.[44]

HRTEM investigation of BTO–ZrO_2 nanocomposite films

Transmission electron microscopy (TEM) bright-field imaging shows the crystallographic information, since the Bragg contrast lets crystals appear bright or dark relative to a mean background. Amorphous phases generally only show little contrast variation with respect to the mean background level. A typical example is shown in Fig. 5(a), which illustrates the phase distribution over the film thickness for the exemplarily chosen composition BTO-20Z. Fig. 5(a) is a bright field image exhibiting a quasi-amorphous bottom layer of this film, whereas the top-layer is nanocrystalline in nature with an average grain size ranging from a few nm up to about 50 nm. The high-resolution TEM images (insets in Fig. 5(a)) accordingly show mostly random contrast which is typical for a quasi-amorphous structure in the bottom part and predominantly lattice fringes of nanocrystallites in the top part of the image. Selected area electron diffraction (SAED)-pattern recorded in the respective areas supports this observation.

Ignoring dynamical scattering effects the contrast in a high angle annular dark field (HAADF) image is roughly proportional to the square of the mean local atomic number ("*Z*-contrast"). Scanning transmission electron microscopy-HAADF (STEM-HAADF) images were taken in order to gain chemical information. The STEM-HAADF image (Fig. 5(b)) roughly shows three different intensity regions. The bright regions are expected to contain a higher fraction of heavy elements, the dark regions a higher fraction of light elements. EDS spectra were taken in different areas of the thin film cross-section (labelled A to D) in order to analyse the chemical composition. They are displayed in Fig. 5(c) and (d) for the Zr-K and Ba-L_{23} line respectively. The oxygen concentration remains constant (68 at%) for all areas within the error of quantification. On the contrary the relative fraction of the elements Ba, Zr and Ti differ distinctively. The brightest regions in the STEM-HAADF image (positions B and C) indeed show a relatively higher fraction of Ba compared to Zr and Ti, the darker regions show either more Ti (position A) or Zr (position D). The results clearly demonstrate that the structure of our composite films consists of several distinct pure phases. An exact definite

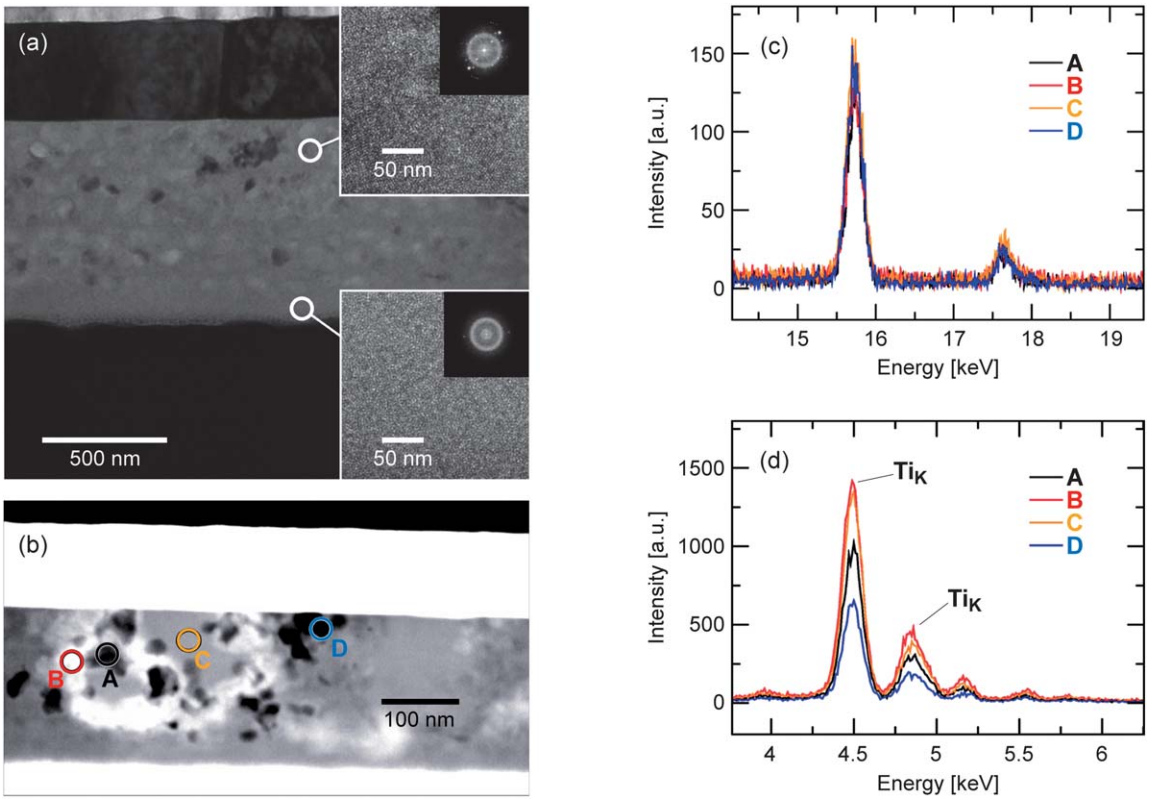

Fig. 5 Transmission-electron microscopy study of a BTO-20Z nanocomposite thin film. (a) Bright field image with high resolution images of the top and the bottom part of the film and the respective SAED-patterns. (b) *Z*-Contrast images by STEM recorded using a HAADF-detector. (c) EDX-spectra recorded using the Zr_K-line for different areas (labelled A to D) of the thin film cross-section. (d) EDX-spectra recorded using the Ba_{L23}-line for different areas (labelled A to D) of the thin film cross-section.

identification of these phases with the methodology chosen here is not possible yet, but it is plausible to assume that the phase located at A or D represents the Zr-rich precipitates, whereas regions like B and C essentially consist of the Ba-rich perovskite phase.

Dielectric properties of BTO–ZrO_2 composite films

The dielectric constant of BTO films is systematically reduced with increasing ZrO_2 contents. This is in fact expected because pure ZrO_2 has a much lower dielectric constant compared to $BaTiO_3$. Additionally the frequency dispersion of the dielectric constant is also reduced with increasing ZrO_2 contents. All these Zr containing films exhibit low loss tangent values irrespective of the probed frequency (see ESI†). The dielectric tunability values, *i.e.* the change of dielectric constant with the applied dc bias voltage, of the BTO-Z composite films are also reduced with increasing ZrO_2 contents and the dielectric constants of BTO-Z films with 30.0 and 40.0 wt% ZrO_2 are almost independent of the applied dc bias voltage (see ESI†). The temperature dependence of the dielectric constant and of the loss tangent of BTO films with various ZrO_2 contents is shown in Fig. 6. Pure BTO itself shows a broad dielectric anomaly. However, this broad dielectric anomaly flattens out with increasing ZrO_2 content, and finally BTO-40Z films exhibit a temperature independent dielectric constant in a wide range of temperatures (−174 to +200 °C). Such a flat dielectric response is extremely desirable in many practical device applications including MLCC and voltage tunable frequency agile microwave electronic (FAME) devices. All films maintain small dielectric loss tangents in the measured temperature range (Fig. 6(b)).

Proposed mechanism for phase and morphology development for the hybrid solution derived films

As mentioned earlier, microemulsion mediated synthesis of barium titanate films results in dielectric properties that are attractive to MLCC applications. Additionally, compared to economic chemical solution derived films, the microemulsion

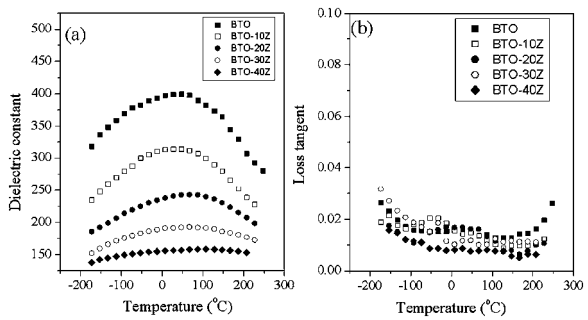

Fig. 6 Temperature dependent (a) dielectric constant and (b) loss tangent of BTO films with various ZrO_2 contents measured at 10 kHz.

mediated route allows to deposit thicker films per coating/firing cycle significantly reducing the processing cost. In the barium titanate:zirconia composite thin films the dielectric constant becomes more and more insensitive to the measurement frequency, dc bias voltage and temperature with progressing increase of the zirconia content. All these material characteristics are attractive for the use of such composite thin films in miniaturized multilayered ceramic capacitors. The relatively low sensitivity of the measured dielectric constant as a function of frequency, dc bias voltage and temperature can be understood in terms of the formation of a heterogeneous 'core–shell' granular microstructure in BTO-Z composite thin films.

The formation of a core–shell type structure has been reported in bulk BTO ceramics doped with rare earth oxides, zirconia, and tantalum oxide. In the case of bulk ceramics, the core consists of undoped (or lightly doped) BTO (ferroelectric with domain structure) with T_c >room temperature while the shell typically is heavily doped (usually paraelectric) with T_c occasionally less than room temperature. The formation of the core–shell structure in bulk BTO ceramics is related to the appearance of an eutectic liquid phase-mixture at sintering temperatures as high as 1370 °C. The binary eutectic temperature for $BaO:TiO_2$ (50 : 50) is reported to be ~1320 °C which is further lowered with the addition of dopant oxides (such as ZrO_2). Upon cooling the undissolved barium titanate forms the core and the liquid (rich in dopant contents) nucleates on the BTO core to form the shell structure. For this reason the shell region crystallizing at the core–shell interface is rich in dopant contents. This dopant concentration is gradually reduced towards the barium titanate core away from the core–shell interface. The structure of the interface between the core and the shell is semi-coherent with associated dislocations due to the lattice mismatch between both phases. Depending on the combination of dwelling-time and sintering temperature solid state diffusion of the dopant takes place from the shell towards the core region resulting in an inhomogeneous distribution of the dopant cation in the shell and core region. The inhomogeneous distribution of the dopant locally shifts the Curie temperature proportionally to the dopant concentration. The superposition of these individual Curie peaks arising from the inhomogeneous distribution of dopants eventually leads to an almost temperature independent dielectric response. Too high sintering temperatures or too long sintering times lead to a homogeneous distribution of the dopant cations causing the reappearance of the single dielectric anomaly that corresponds to the paraelectric to ferroelectric phase transition with a reduced transition temperature as compared to the bulk BTO ceramics.[45]

The formation mechanism of the core–shell structure in the present BTO-Z composite films is distinctly different from its bulk counterpart because no liquid phase is expected to exist at the annealing temperatures applied in this study (700–800 °C). A plausible mechanism for the core–shell microstructure in BTO-Z films is presented as follows. As illustrated in Fig. 7(a), our microemulsion derived dispersions consist of a solvent mixture of cyclohexane and methanol, in which BTO nanoparticles are stabilized by a cationic surfactant with a polar hydrophilic head and a long aliphatic chain tail in the oil phase. The hybrid solutions used here consisted of mixtures of these BTO suspensions and acetylacetone stabilized $Zr(O^nBu)_4$ as a Zr-precursor. Usually the hydrolysis reaction of pure $Zr(O^nBu)_4$ consists several major steps. First the OH ligands substitute an OR molecular group. In a second step hydroxo ligands separate from the complex together with another alkoxy group to create Zr–O–Zr bonds. These two steps as described above are repeated

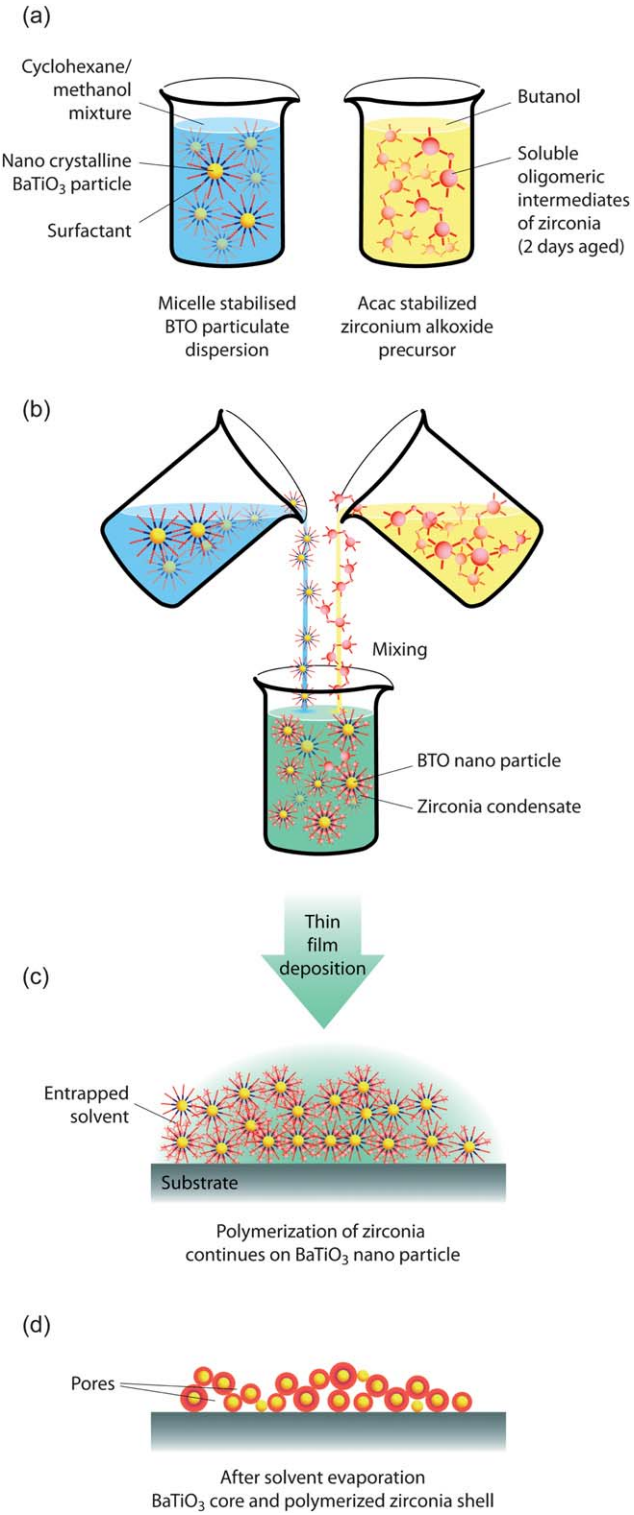

Fig. 7 Plausible mechanism for the core–shell microstructure in the BTO–ZrO_2 composite films (see text for details).

to replace the remaining two OR groups of the initial alkoxide eventually forming metazirconic acid, $(ZrO_2)_n \cdot mH_2O$ depending on the available water content. Since this hydrolysis reaction is much quicker than the condensation process the solid phase obtained consists of dense hydrated aggregates of zirconium oxide. In order to produce soluble polymeric intermediates, it was necessary to slow down the hydrolysis reaction. This was achieved by complexing the Zr-*n*-butoxide through the introduction of acetylacetone into the butanol solution as a chelating additive. The solution was aged in a separate beaker for a couple of days to form zirconia oligomers. The two precursors in separate beakers (Fig. 7(a)) were mixed together to form a microemulsion–alkoxide hybrid sol (Fig. 7(b)). As shown, zirconia oligomers are dispersed in the organic micelle walls of BTO core particle to form a core–shell structure in the hybrid precursor sol.

Mainly two different types of mechanism have been invoked in the literature to explain the formation of nano-crystalline core–shell structures *via* the reverse micelle route.[46] Direct experimental evidence for any of these two mechanisms remains scanty due to the non-availability of suitable characterization tools allowing for the direct observation of the phenomena occurring when the shell is formed on the core of the particle. The first mechanism proposed is based on ionic substitution. As an illustrative example of this mechanism, the addition of Ag^+ cations to a microemulsion containing cadmium sulfide (CdS) is considered.[46] Here the added Ag^+ cations partially replace Cd^{2+} ($2\ Ag^+ + CdS \rightarrow Cd^{2+} + Ag_2S$) resulting in a monolayer shell of silver sulfide (Ag_2S) on a core of CdS. Such an ionic displacement reaction is not always energetically favorable. For example the formation of a ZnS shell on a CdS core by ionic exchange has a positive value of the associated Gibbs free energy change and therefore does not occur in practice. Another possible mechanism is the heterogeneous nucleation and subsequent growth of a shell layer on the core particles. The mechanism of heterogeneous nucleation is reported to form thicker shell layers compared to the layer growth by ionic exchange. According to this mechanism, the CdS particle acts as a heterogeneous site for the nucleation and subsequent growth of a surrounding Ag_2S shell.[46]

The ionic exchange mechanism can be ruled out in our case because it is not possible to have Zr^{4+} ions separated from the acetylacetone stabilized zirconia oligomers in the hybrid precursor sol. The steric strain of the chelated alkoxide is much larger than that of the non-chelated Zr alkoxide resulting in a slower hydrolysis reaction of the former species compared to the latter one. This slower hydrolysis reaction is expected to yield a linear gel type structure upon condensation. Mainly due to Coulombic attraction, the zirconia oligomers are flocked in the vicinity of the surfactant stabilized BTO core to form a core–shell structure in the hybrid sol. This has been depicted schematically in Fig. 7(b). Similar emulsion polymerization of a monomer species has also been reported in the literature. For example, Sanchez and In[47] reported the polymerization of a methylmethacrylate monomer onto TiO_2 particles occupying the cores of micelles resulting in the formation of a core–shell hybrid material in the mixed precursor sol. Our hybrid sol was spin coated onto platinized silicon substrates (Fig. 7(c)). The core–shell structures of the hybrid sol come into close proximity in the deposited film with the oil phase, surfactant, and the solvent trapped in between. At this stage the polymerization of zirconia on BTO core particles continues. Depending on the concentration of oligomers surrounding the BTO cores in the hybrid sol, which is determined by the alkoxide content of the hybrid sol, the thickness of the shell is varied around each core particle. Accordingly some of the core particles may not have any condensed shell on their surface. Just after deposition the composite films were directly inserted into a preheated furnace kept at 700 °C and heat treated for 10 minutes. At this temperature solvent, oil phase as well as the surfactants are evaporated instantaneously and a zirconia shell forms as an oxide skeleton on the BTO core. Fig. 7(d) illustrates this situation just after organic removal. The film has a porous microstructure at this stage and each BTO core is surrounded by a zirconium oxide based shell layer with varying thicknesses. When sintering proceeds, Zr^{4+} ions from the reactive oxide skeleton of the shell diffuse, driven by the concentration gradient, inwards to the BTO core. Due to the unequal thickness of the shell layer, the said concentration gradient varies from BTO core to BTO core. Since the annealing temperature and time are kept relatively low (700 °C and 10 minutes, respectively) the diffusion rate of the dopant is slow along the relatively short diffusion paths (corresponding to the radius of the core particle). The slow diffusion rate of the dopant cation in turn consequently would yield in an inhomogeneous dopant distribution within as well as between the BTO grains.

In view of this proposed model the structural as well as electrical characteristics of the BTO-Z composite film as described above can easily be understood. The nanoscale Ti:Zr compositional heterogeneity is reflected through XRD patterns, Raman-spectra and the thorough TEM-analysis of the BTO-Z composite thin films. It is worthwhile to note that even at high zirconia contents, as for example in BTO-40Z composite films, no diffraction peak corresponding to any of the known ZrO_2 polymorphs could be detected. This indicates that ZrO_2 is not phase separated in the composite films. There is no systematic shift of the diffraction peaks of BTO with a progressive increase in ZrO_2 contents (Fig. 7(a)). Since the Zr^{4+} cation has a larger ionic radius than Ti^{4+} (72 pm *vs.* 60.5 pm), it would increase the lattice constant of BTO resulting in a shift of the respective diffraction peaks towards lower 2θ values, if Zr is incorporated into the perovskite lattice. The absence of any such systematic shift of the diffraction peaks in BTO-Z films with increasing ZrO_2 contents supports the compositional heterogeneity model described above. In the same way our results obtained by Raman-scattering support the assumption that Zr is not or only very little incorporated into the BTO lattice, since no variation of phonon frequencies and herewith of force-constants could be confirmed.

The compositional heterogeneity is also reflected in the measured dielectric properties in terms of a minimal change of the dielectric constant as a function of temperature that yields a flat dielectric response in BTO-Z films with higher (>20%) zirconia contents. Neither a shift of the positions for the Bragg-reflections in XRD nor a significant change of their full width at half maximum (FWHM) could be detected. The FWHM values correspond to the grain size observed in the films and are typical for free nanocrystalline $BaTiO_3$ particles of comparable dimensions.[27]

The model described above may also be applied to explain the interesting findings of the morphology selection during processing of *BTO:BTO hybrid solutions* discussed in the corresponding section (*vide supra*). In order to do this one has to take into account that at first nucleation has to occur and then these nuclei typically grow during further thermal treatment, *i.e.* the models for the standard nucleation theory from glasses can be utilized and adapted.[48] Eqn (2) and (3) describe the free energy barriers of homogeneous (ΔG^*_{homo}) and heterogeneous (ΔG^*_{hetero}) nucleation, respectively.

$$\Delta G^*_{homo} = \frac{16\pi\gamma^3}{3(\Delta G_v)^2} \quad (2)$$

$$\Delta G^*_{hetero} = \frac{16\pi\gamma^3}{3(\Delta G_v)^2} f(\theta) \quad (3)$$

where γ is the interfacial energy and ΔG_v is the driving force for crystallization *i.e.* the free energy difference per unit volume for the amorphous–crystalline film transformation, and $f(\theta)$ is a function related to the contact angle. Basically columnar growth requires the dominance of the heterogeneous over the homogeneous nucleation events. This is typically the case for thin film materials like lead zirconate titanate (PZT)[49] but normally not for alkaline earth titanates like BTO.[50,51] They tend to nucleate homogeneously within the volume of the film as long as the thickness of the as-deposited film is larger than approx. 10–15 nm[31] leading to a fine grained morphology. Consequently this trend is also observed in the amorphized and subsequently re-crystallized BST films mentioned above.[36]

Only if the film thickness of the as deposited *con*-BTO film is around 10 nm per coating, directly followed by crystallization in the diffusion furnace heterogeneous nucleation events at the electrode–film interface are preferred leading to a columnar growth. The disadvantage however is the large number of coatings required for thicker films as already pointed out. The situation changes if the *BTO:BTO hybrid solutions* are employed. In analogy to the development of a core–shell type structure of the zirconia precursor around the amorphous μE-BTO nanoparticle, described above, we postulated that also the propionate based BTO precursor forms such a shell around the amorphous μE-BTO nanoparticle. Depending on the amount of *con*-BTO this shell is more or less complete. This *con*-BTO precursor typically decomposes *via* an intermediate alkaline earth carbonate or oxo-carbonate phase which is stable up to 600–650 °C[29,52,53] and can basically act as a nucleation seed. Simultaneously also the amorphous μE-BTO grains do not crystallize below 600 °C.

A comparison to results from the PZT system gives further hints. Schwartz *et al.*[48] have shown that PZT precursors which possess higher decomposition temperatures usually have a stronger tendency for heterogeneous nucleation. Higher decomposition temperatures lead to reduction in the free energy for crystallization and driving force for crystallization, respectively. Since this free energy difference defines the barrier height for homogeneous nucleation within the bulk of the film as well as the barrier height for the heterogeneous nucleation at the interface any change in the driving force (ΔG_v) will impact the relative barrier heights, for these different nucleation events. In a modified form this might be applied to the present BTO system. The addition of more and more propionate based *con*-BTO solution to the colloidal μE-BTO nanoparticle dispersion increases the decomposition (crystallization) temperature due to the presence of intermediate carbonates in the tiny shell around the μE-BTO nanoparticles during thermal treatment. Hence the barriers for homogeneous nucleation increase due to decrease of ΔG_v. At the same time ΔG^*_{hetero} can also change but the function $f(\theta)$ probably changes only slightly in a way that $\Delta(\Delta G^*_{homo} - \Delta G^*_{hetero})$ always increases to a larger extent with increase of the *con*-BTO content in the hybrid solution. This is schematically shown in Fig. 8.

At this point it has to be mentioned that the ΔG^*_{homo} and ΔG^*_{hetero} nucleation could change for each of the hybrid solutions. In order to simplify the situation in the present qualitative model ΔG^*_{hetero} for heterogeneous nucleation has been assumed to be approx. constant (Fig. 8). Taking this into account under a constant temperature ramp at any particular moment the greater the free energy difference between the homogeneous and heterogeneous nucleation the larger the dominance of the interface nucleation. From the thermodynamic point of view films with larger *con*-BTO content therefore have an increased propensity towards nucleating at the Pt/BTO film interface forming columnar grains. However this cannot solely explain our finding that only in the RTA (higher heating ramp compared to the diffusion furnace) columnar grown films can be obtained. In order to find a possible explanation one has also to take into account that in the case of the *con*-BTO typically formed intermediate oxo-carbonate grains may act as nucleation seeds for the BTO–perovskite grains. This means that also kinetic aspects which are based on the nucleation and growth rates of the two different events control the film formation process in the

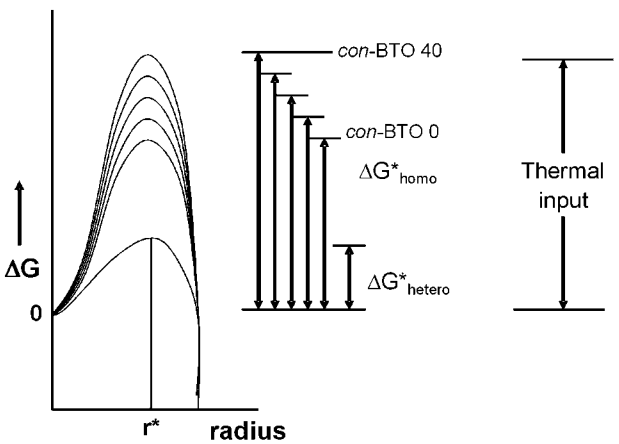

Fig. 8 Schematic for the hypothetical change of free energy barriers for homogeneous (ΔG^*_{homo}) and heterogeneous (ΔG^*_{hetero}) nucleation depending on the amount of *con*-BTO addition to the μE-BTO dispersion. r^* represents the critical radii for nuclei growth. As indicated in the text the barrier height for ΔG^*_{hetero} is kept constant to simplify the diagram. Besides the different barrier heights on the right hand side the amount of available thermal energy input is plotted. In the case of *con*-BTO 40 the latter is barely sufficient to surmount the energy difference for the homogeneous nucleation. Thus depending on the kinetics a columnar (Fig. 2d, RTA process) and a polycrystalline (diffusion furnace), respectively, morphology is obtained.

con-BTO/μE-BTO system. In order to explain this it may be assumed that in the case of fast heating (RTA) the formation of this oxo-carbonate phase is significantly delayed to higher temperatures, where the thermal input is already high enough for the crystallization of BTO. If the admixture of *con*-BTO reaches 40% (Fig. 8) however the thermal input is only sufficient for heterogeneous nucleation at the interface and the oxo-carbonate phase might be not fully formed in the whole volume of the film yet. Simultaneously the temperature is already high enough to enable the quick growth of the initially formed BTO nuclei at the interface hence winning the competition against the possible nucleation events at the oxo-carbonate grains within the volume of the film, leading to an overall columnar grown BTO-film in this case.

3 Experimental details

Synthesis of BTO nanoparticle dispersion, molecular precursor solution, and hybrid solutions

Water in oil type reverse micelles (microemulsions) were used as nano-reactors to synthesize nano-crystalline BT particles. A brief outline of the preparation process is given here and further details of it may be found elsewhere.[20,26] The approach relies on the hydrolytic decomposition of a mixed Ba-Ti-methoxide solution in reverse micelles water nano-pool. The composition of a typical microemulsion was 12.21 wt% 1-pentanol, 3.74 wt% CTAB, 11.23 wt% ultrapure degassed and Ar saturated water and 72.82 wt% cyclohexane. After the preparation of the metallo-organic double alkoxide of Ba-Ti by dissolving Ba-metal in methanol and adding Ti-isopropoxide to the reaction mixture, a stoichiometric amount of the microemulsion was added dropwise at room temperature. This leads to the formation of a homogeneous dispersion of nano-crystalline $BaTiO_3$ particles with surfactant molecules adsorbed at the surface. The concentration of the optically transparent precursor sol, diluted with methanol, is estimated to be approx. 0.17 mol l^{-1}. The typical particle size of the nano-crystalline BTO, determined by dynamic light scattering using a Malvern Zetasizer, is estimated to be 5 ± 0.5 nm. The stable nanoparticle dispersion prepared in this way was used directly for the deposition of BTO thin films. In order to reduce the porosity and to increase the reliability of the dielectric layers, the micro-emulsion mediated particulate sol containing 5% BT was mixed with a molecular BTO alkoxide (0.17 mol l^{-1}) solution, prepared using barium propionate and titanium tetra-*n*-butoxide according to ref. 31 and 54. The volume contents of BT alkoxide in the microemulsion:alkoxide hybrid sol were varied in the range of 0.0 to 40 volume percent. To prepare the microemulsion BTO:alkoxide zirconia hybrid precursor sol, zirconium tetra-*n*-butoxide was used as an alkoxide precursor. The concentration of the alkoxide precursor solution was maintained constant at 0.17 mol l^{-1}. For this purpose the Zr-alkoxide was dissolved in *n*-butanol and 2 mol acetylacetone were used as a stabilizing agent to reduce the moisture sensitivity (slow down the hydrolysis reaction) of the Zr-precursor solution. To prepare the hybrid precursor solution stoichiometric amounts of Zr alkoxide precursor solution and BTO nanoparticle dispersion were carefully mixed together to yield in 0.0, 1.0, 5.0, 10.0, 20.0, 30.0, and 40.0 wt% ZrO_2 in the final nanocomposite film. Before mixing the Zr-alkoxide with the BTO particulate sol, the alkoxide solution needs to be aged for 2–3 days to stabilize the hybrid solution.

Film preparation

All films were deposited in a class 1000 clean room on a B.L.E Delta 20 photoresist spin-coater after purging with dry nitrogen starting with a rotation speed of 500 rpm for 5 s followed by 4000 rpm for 30 s. Just after deposition, the films were directly inserted in a preheated diffusion furnace (ramp rate $\sim$10 K s^{-1}) or an AST RTA (with an averaged ramp rate of $\sim$56 K s^{-1}) and annealed at temperatures in the range of 700–800 °C for 10–30 minutes in ambient oxygen, respectively. Suitable heat treatment schedules have been selected according to the decomposition behavior described in the Results and discussion section. The coating and firing schedule was repeated for 1–4 times to yield films of about 200–580 nm thickness.

Morphological characterisation

The surface as well as the cross-section morphology of the annealed films was studied by field emission scanning electron microscopy using a Zeiss DSM 982 Gemini instrument. X-Ray diffraction patterns using glancing angle were recorded with a Philips X-Pert system with Cu-K_α radiation, $\lambda = 1.5405$ Å, to characterize the phase formation behavior of the annealed films. The structural analyses of the annealed films were performed using XRD in conjunction with confocal micro-Raman (Horiba Yvon T64000) scattering measurements.

Samples for investigations by high resolution transmission electron microscopy (HRTEM) were prepared by focused ion beam (FIB) milling in a ZEISS (LEO) 1540XB dual beam FIB. TEM measurements were performed in a FEI Tecnai F20 instrument at an acceleration voltage of 200 kV. Scanning transmission electron microscopy (STEM) "*Z*-contrast" images were taken with a Fischione Model 3000 high-angle annular dark-field detector. Energy dispersive X-ray spectra were recorded with an EDAX Phoenix system.

Electrical characterisation

A metal–insulator–metal (MIM) parallel plate capacitor structure was used for the electrical measurements of the annealed films. For this purpose circular platinum top contacts (approximately 200 μm in diameter) were deposited on the film surface and parts of the films were chemically etched to expose the underlying platinum layer as bottom contact. The dielectric properties of the annealed films were measured as a function of frequency (100 Hz to 100 kHz) and temperature (RT–350 °C). A commercial probe station equipped with a computer controlled thermal stage was used for all the electrical measurements. A HP 4294A impedance analyzer was used to measure the dielectric properties. The equipment was addressed remotely *via* IEEE488 GPIB bus, for automatic control of the measurement process parameter and for data acquisition.

4 Conclusions

In the present work by means of stabile BTO nanoparticle dispersions derived from microemulsion mediated synthesis the

potential for ceramic nanocomposite thin film fabrication has been evaluated. At first films prepared from pure reverse micelles derived BTO nanoparticle dispersions have been investigated. Hence after annealing at 750 °C crystalline, fine grained BTO films with an average grain size of approximately 30 nm have been obtained. The dielectric constant and loss tangent of these BTO films measured at 1 kHz were 406 and 0.013, respectively, which compare well with former BTO thin films obtained by classical CSD routes featuring a comparable microstructure but requiring a larger number of coating steps. In order to increase the density of the BTO films mentioned above and moreover to develop a tool for the introduction of a tailored heterogeneity on the nanoscale and a nanocomposite, respectively, the novel concept of "*hybrid solutions*" has been introduced. These hybrid precursor sols consist of various mixtures of stoichiometric amounts of conventional CSD precursor solutions and microemulsion derived BTO nanoparticulate sols.

In the first case *i.e.* the admixture of various amounts of conventional BTO precursor solutions to the BTO nanoparticle dispersion it has been observed that the microstructure can be controlled by a combination of the amount of admixed *con*-BTO to the *μE*-BTO and the heating ramp. Relatively high amounts of *con*-BTO (40 vol%) and steep heating ramps (~56 K s^{-1}) facilitate a columnar growth, while smaller amounts and moderate heating ramps (~10 K s^{-1}) lead to more grainy microstructures. In accordance with the literature the approx. 200 nm thick columnar grown BTO films show superior permittivities of up to 1050 in the case of *con*-BTO 40. The salient feature of this approach is that only 25% of the number of coating steps of standard CSD processing for BTO is required to achieve the same properties. In order to explain the observed microstructure evolution a qualitative model consisting of a combination of modified glass nucleation theory and kinetic aspects was presented.

In the second example barium titanate:zirconia nanocomposite films were synthesized using the *hybrid solution* approach. Thus various mixtures of a conventional zirconium alkoxide based precursor solution (*con*-ZrO_2) and the *μE*-BTO dispersion have been prepared yielding in nanocomposite BTO-Z thin films with 1.0, 5.0, 10.0, 20.0, 30.0, and 40.0 wt% ZrO_2, respectively. The dielectric constant as well as loss tangent dispersions as a function of frequency, dc voltage and temperature were found to be markedly reduced with increasing ZrO_2 contents in BTO-Z composite thin films. The observed dielectric properties have been explained in terms of their nanoscale compositional heterogeneity (Ti/Zr ratio), which was modeled in terms of the formation of a ZrO_2 oligomer shell on a nanocrystalline BTO core in the *hybrid precursor sol*. Upon annealing, the aimed compositional heterogeneity of the initial *hybrid coating solution* is maintained until the final crystalline BTO–ZrO_2 nanocomposite film is formed. No hints for BTZ solid solution formation have been found and the aimed nanoscale compositional heterogeneity was confirmed by Raman spectroscopy, XRD, and a thorough HRTEM study, by which the heterogeneity on the nanoscale was directly visualized and analyzed by STEM-HAADF.

Overall on the basis of the model system BTO–ZrO_2 a novel approach has been presented for the fabrication of nanocomposite ceramic thin films which might be able to close the gap between conventional powder based fabrication routines (films down to ~0.8 μm) and classical thin film techniques (typically up to ~300 nm) for composite films with a tailored nanoscale heterogeneity for applications like MLCC's. Moreover the principle of *hybrid solutions* may also be applied for other material systems where a nanoscale heterogeneity of the functional thin film is required.

Acknowledgements

The research described in this publication was supported by the Deutsche Forschungsgemeinschaft within the priority program SPP1181. S. B. Majumder wishes to thank Alexander von Humboldt foundation for the partial financial support to carry out the research work and N. Vyshnavi acknowledges the financial support rendered by the DAAD sandwich Fellowship. Thomas Pössinger is acknowledged for preparing the artwork.

References

1 D. F. K. Hennings, *J. Eur. Ceram. Soc.*, 2001, **21**, 1637.
2 S. Sato, Y. Nakano, A. Sato and T. Nomura, *J. Eur. Ceram. Soc.*, 1999, **19**, 1061.
3 H. Kishi, Y. Mizuno and H. Chazono, *Jpn. J. Appl. Phys.*, 2003, **42**, 1.
4 X. Liu, S. Cheng and C. A. Randall, *J. Korean Phys. Soc.*, 1998, **32**, S312.
5 M. Randall, D. Skamser, T. Kinard, J. Qazi, A. Tajuddin, S. Trollier-Mc Kinstry, C. Randall, S. W. Ko and T. Dechakupt, *Thin Film MLCC, CARTS 2007 Symposium Proceedings, Albuquerque, NM, 2007*, Electronic Components, Assemblies & Materials Association (ECA), Arlington, VA, 2007.
6 R. W. Schwartz, T. Schneller and R. Waser, *C. R. Chim.*, 2004, **7**, 433.
7 M. Grossmann, R. Slowak, S. Hoffmann, H. John and R. Waser, *J. Eur. Ceram. Soc.*, 1999, **19**, 1413.
8 Y. Sakabe, Y. Takeshima and K. Tanaka, *J. Electroceram.*, 1999, **3** (2), 115.
9 L. Huang, Z. Chen, J. D. Wilson, S. Banerjee, R. D. Robinson, I. P. Herman, R. Laibowitz and S. O'Brien, *J. Appl. Phys.*, 2006, **100**, 034316.
10 J. Xu, J. Zhai and X. Yao, *Appl. Phys. Lett.*, 2006, **89**, 252902.
11 Y. Yamashita, H. Yamamoto and Y. Sakabe, *Jpn. J. Appl. Phys.*, 2004, **43**, 6521.
12 A. Li, C. Ge, P. Lü, D. Wu, S. Xiong and N. Ming, *Appl. Phys. Lett.*, 1997, **70**, 1616.
13 A. Rüdiger, T. Schneller, A. Roelofs, S. Tiedke, T. Schmitz and R. Waser, *Appl. Phys. A: Mater. Sci. Process.*, 2005, **80**, 1247.
14 T. Ohno, D. Suzuki, H. Suzuki and T. Ida, *J. Soc. Powder Technol. Jpn.*, 2004, **41**, 86.
15 Y. Shiratori, C. Pithan, J. Dornseiffer and R. Waser, *J. Raman Spectrosc.*, 2007, **38**, 1288.
16 Y. Shiratori, C. Pithan, J. Dornseiffer and R. Waser, *J. Raman Spectrosc.*, 2007, **38**, 1300.
17 S. Wohlrab, M. Weiss, H. Du and S. Kaskel, *Chem. Mater.*, 2006, **18**, 4227.
18 C. Pithan, D. Hennings and R. Waser, *Int. J. Appl. Ceram. Technol.*, 2005, **2**, 1.
19 M. Niederberger, G. Garnweitner, N. Pinna and M. Antonietti, *J. Am. Chem. Soc.*, 2004, **126**, 9120.
20 C. Pithan, T. Schneller, Y. Shiratori, S. B. Majumder, F.-H. Haegel, J. Dornseiffer and R. Waser, *Int. J. Mater. Res.*, 2006, **97**, 5.
21 T. Ahmad, G. Kavitha, C. Narayana and A. K. Ganguli, *J. Mater. Res.*, 2005, **20**, 1415.
22 J. Wang, J. Fang, S. C. Ng, L.-M. Gan, C.-H. Chew, X. Wang and Z. Shen, *J. Am. Ceram. Soc.*, 1999, **82**, 873.
23 C. Beck, W. Härtl and R. Hempelmann, *J. Mater. Res.*, 1998, **13**, 3174.
24 V. Chhabra, V. Pillai, B. K. Mishra, A. Morrone and D. O. Shah, *Langmuir*, 1996, **11**, 3307.
25 H. Herrig and R. Hempelmann, *Mater. Lett.*, 1996, **27**, 287.

26 T. Schneller, C. Pithan, J. Dornseiffer, F.-H. Hägel and R. Waser, 2006, DE 102006025770.7.
27 C. Pithan, Y. Shiratori, R. Waser, J. Dornseiffer and F.-H. Haegel, *J. Am. Ceram. Soc.*, 2006, **89**, 2908.
28 S. Halder, T. Schneller and R. Waser, *Mater. Res. Soc. Symp. Proc.*, 2004, **811**, D3.30.1.
29 U. Hasenkox, S. Hoffmann and R. Waser, *J. Sol-Gel Sci. Technol.*, 1998, **12**, 67.
30 Y. Ding, C. Jin and Z. Meng, *Thin Solid Films*, 2000, **375**, 196.
31 S. Hoffmann and R. Waser, *J. Eur. Ceram. Soc.*, 1999, **19**, 1339.
32 D. Hennings, G. Rosenstein and H. Schreinemacher, *J. Eur. Ceram. Soc.*, 1991, **8**, 107.
33 A. Lotnyk, S. Senz and D. Hesse, *Solid State Ionics*, 2006, **177**, 429.
34 A. Mosset, I. L. Gautier-Luneau, J. Galy, P. Strehlow and H. Schmidt, *J. Non-Cryst. Solids*, 1988, **100**, 339.
35 S. Halder, T. Schneller and R. Waser, *J. Sol-Gel Sci. Technol.*, 2005, **33**, 299.
36 R. Liedtke, S. Hoffmann and R. Waser, *J. Am. Ceram. Soc.*, 2000, **83**, 436.
37 G. Datta, H. S. Maiti and A. Paul, *J. Mater. Sci. Lett.*, 1987, **6**, 787.
38 S. K. Sahoo, D. C. Agrawal, Y. N. Mohapatra, S. B. Majumder and R. S. Katiyar, *Appl. Phys. Lett.*, 2004, **85**, 5001.
39 M. Jain, S. B. Majumder, R. S. Katiyar, D. C. Agrawal and A. S. Bhalla, *Appl. Phys. Lett.*, 2002, **81**, 3212.
40 M. Jain, S. B. Majumder, R. S. Katiyar, F. A. Miranda and F. W. Van Keuls, *Appl. Phys. Lett.*, 2003, **82**, 1911.
41 V. G. Keramidas and W. B. White, *J. Am. Ceram. Soc.*, 1974, **57**, 22.
42 P. Barberis, T. Merle-Méjean and P. Quintard, *J. Nucl. Mater.*, 1997, **246**, 232.
43 J. C. Debsikdar, *J. Non-Cryst. Solids*, 1986, **87**, 343.
44 S. Halder, T. Schneller, U. Böttger and R. Waser, *Appl. Phys. A: Mater. Sci. Process.*, 2005, **81**, 25.
45 H. Y. Lu, J. S. Bow and W.-H. Deng, *J. Am. Ceram. Soc.*, 1990, **73**, 3562.
46 D. Shukla and A. Mehra, *Langmuir*, 2006, **22**, 9500.
47 C. Sanchez and M. In, *J. Non-Cryst. Solids*, 1992, **147/148**, 1.
48 R. W. Schwartz, J. A. Voigt, B. A. Tuttle, D. A. Payne, T. L. Reichert and R. S. DaSalla, *J. Mater. Res.*, 1997, **12**, 444.
49 M. J. Lefevre, J. S. Speck, R. W. Schwartz, D. Dimos and S. J. Lockwood, *J. Mater. Res.*, 1996, **11**, 2076.
50 T. Hayashi, N. Oji and H. Maiwa, *Jpn. J. Appl. Phys.*, 1994, **33**, 5277.
51 M. C. Gust, L. A. Momoda and M. L. Mecartney, *Mater. Res. Soc. Symp. Proc.*, 1994, **346**, 649.
52 H. S. Gopalakrishnamurthy, M. Subba Rao and T. R. Narayana Kutty, *J. Inorg. Nucl. Chem.*, 1975, **37**, 891.
53 D. Hennings, G. Rosenstein and S. Schreinemacher, *J. Eur. Ceram. Soc.*, 1991, **8**, 107.
54 S. Halder, T. Schneller, R. Waser and F. Thomas, *J. Sol-Gel Sci. Technol.*, 2007, **42**, 203.